JMEPEG (2009) 18:424–432
DOI: 10.1007/s11665-008-9227-3

1059-9495/$19.00

Relationships Between Abrasive Wear, Hardness, and Grinding Characteristics of Titanium-Based Metal-Matrix Composites

Peter J. Blau and Brian C. Jolly

(Submitted January 28, 2008)

The objective of this work was to support the development of grinding models for titanium metal-matrix composites (MMCs) by investigating possible relationships between their indentation hardness, low-stress belt abrasion, high-stress belt abrasion, and the surface grinding characteristics. Three Ti-based particulate composites were tested and compared with the popular titanium alloy Ti-6Al-4V. The three composites were a Ti-6Al-4V-based MMC with 5% TiB_2 particles, a Ti-6Al-4V MMC with 10% TiC particles, and a Ti-6Al-4V/Ti-7.5%W binary alloy matrix that contained 7.5% TiC particles. Two types of belt abrasion tests were used: (a) a modified ASTM G164 low-stress loop abrasion test, and (b) a higher-stress test developed to quantify the grindability of ceramics. Results were correlated with G-ratios (ratio of stock removed to abrasives consumed) obtained from an instrumented surface grinder. Brinell hardness correlated better with abrasion characteristics than microindentation or scratch hardness. Wear volumes from low-stress and high-stress abrasive belt tests were related by a second-degree polynomial. Grindability numbers correlated with hard particle content but were also matrix-dependent.

Keywords machining, metal matrix composites, titanium

1. Introduction

Grinding is basically a controlled abrasive wear, so it is reasonable to expect that there would be a correlation between the abrasive wear of a material, its properties that relate to abrasive wear, and it grindability. However, this relationship is not only a function of material properties. When a material is ground, the rate of removal depends on the properties and characteristics of the material, the abrasive media, the coolant (if used), and the grinder. In effect, machining processes impose energy to do work on a solid body, the net result of which is to change the body's shape or surface finish by removing a desired volume of material. Energy is dissipated in a variety of ways, including the generation of heat, deformation and fracture, sound, and other vibrations.

Empirical models for grinding contain factors that attempt to consolidate variables that are not named explicitly, but these factors can have equal or greater influence than those explicitly taken into account. For example, past work on the grinding of ceramics highlighted the importance of the machine stiffness (Ref 1, 2). Thus, the materials and the machine interact in ways that either enhance removal rate or reduce it. As Malkin points out (Ref 3), knowing where the energy goes in the overall grinding process is a key to its fundamental understanding.

Peter J. Blau and **Brian C. Jolly**, Materials Science and Technology Division, Oak Ridge National Laboratory, P.O. Box 2008, M/S 6063, Oak Ridge, TN 37831-6063. Contact e-mail: blaupj@ornl.gov.

Nomenclature

a	in grindability testing, the length of the ground face (mm)
A	in loop abrasion testing, the nominal contact area (mm^2)
b	in grindability testing, the width of the ground face (mm)
c	in loop abrasion testing, the width of the specimen (mm)
El	elongation in tensile testing (%)
F_n	normal force during grinding (N)
F_x	tangential force during grinding (N)
Gr	grindability number (mm^3/N·m)
HBW	Brinell hardness number
HS	scratch hardness number (GPa)
HV	Vickers microindentation hardness (GPa)
k_{th}	thermal conductivity (W/m·K)
L	in grindability testing, the sliding distance (m)
N	in grindability testing, the normal force (N)
PC	concentration of hard particles in a composite (vol.%)
R	in loop abrasion testing, the radius of the pulley below the specimen contact (mm)
R_g	grinding ratio, (V_{gs}/V_{gw}) (dimensionless)
t	time (s)
UTS	ultimate tensile strength (MPa)
v	in grindability testing, the sliding speed (m/s)
V_{gs}	volume of stock removed by grinding (mm^3)
V_{gw}	volume of wheel worn off (mm^3)
w	in loop abrasion testing, the wear scar length (mm)
Δx	in grindability testing, the specimen length change (mm)
y	in loop abrasion testing, the length of the contact arc (mm)
YS	2% off-set yield strength (MPa)
θ	in loop abrasion testing, the wrap angle of the abrasive band over the pulley (radians)
ρ	density (g/cm^3)

Power (work per unit time) is supplied by a motor. Some of this is lost in the bearings and drive system, but most is transmitted to the wheel/workpiece interface. There, the picture becomes more complicated.

To affect the highest material removal rates, as much energy as possible should be dissipated as deformation and fracture of the workpiece material. However, some of that energy is used up in wearing the wheel or overcoming the friction caused by grinding swarf that clogs the space between the exposed grits. Some of the available energy from the wheel is also converted to heat that is removed by the coolant, transmitted to the chips, conducted into the fixtures via the workpiece, or radiated to the surroundings. Depending on the materials and geometric conditions of grinding the partition of energy can change. Thus, the grinding characteristics of a material are dependent on many aspects of the system, and it is naïve to expect that they can be described in terms of material properties alone.

Like grinding, hardness measurements and wear measurements are also influenced by a combination of materials and tribosystem properties. An indentation hardness number is affected by the shape of the indenter, the rate of indentation, the applied force, and the method used to measure the impression (depth-sensing, optical imaging, etc.). Therefore, the hardness number is not a basic property of a material but a quantified response of a surface to the applied testing conditions. The same can be said for abrasive wear with its additional considerations of abrasive media characteristics, surface speed, chemical environment, and more.

If a correlation between laboratory test data for a set of materials and their characteristics on a full-sized surface grinder were to be obtained, then one could quickly screen new materials like ceramics and composites for their machining characteristics. Also, the correlation of hardness and abrasive wear characteristics of a material with its grinding behavior could improve our basic understanding of grindability itself. While the term grindability may be interpreted as the ability of a material to be rapidly ground and still achieve a desired level of surface quality, in the present context, grindability refers to the relative ease by which material can be removed by grinding.

A titanium alloy and three composites based on it were chosen for this work. While Ti alloys have been used extensively for aerospace components, the use of titanium instead of steel or cast iron in ground vehicles has the potential to reduce weight and hence increase fuel economy. Resistance to road de-icing chemicals is another attractive advantage of Ti alloys. Grinding of Ti alloys is problematical because of their toughness and tendency to transfer to tooling or load the grinding wheel. Their relatively low thermal conductivity causes heat to build up in the grinding zone. Okabe et al. (Ref 4, 5) found that in Ti alloys of the $\alpha + \beta$ type, like Ti-6Al-4V, the lower was their tensile ductility and fracture toughness, the better was their grindability. The current MMCs were selected to exhibit a range of mechanical properties that would in turn produce a range in grindability.

To summarize, the objective of this work was to investigate correlations between two types of belt abrasion tests, several types of hardness measurements, and full-scale surface grinding of a popular titanium alloy Ti-6Al-4V and several Ti-based MMCs. The goal in establishing such correlations was to determine whether full-scale grinding behavior could be estimated from coupon-scale laboratory tests or hardness data and to prompt the development of better models for grinding Ti-based materials.

2. Experimental Procedure and Materials

In addition to indentation hardness characterization using several scales, three abrasive conditions were compared: (a) low-stress abrasion by a belt, (b) higher-stress abrasion on a belt-type, grindability testing machine, and (c) surface grinding on an instrumented machine tool.

The loop abrasion tester was used to conduct low-stress, two-body abrasive wear tests in accordance with ASTM G174 (Ref 6). It consists of a continuous loop of bonded abrasive, in this case 30 μm average grit diameter alumina, mounted on three pulleys (see Fig. 1). A 3 mm thick, 8 mm wide, and 25 mm long, rectangular test specimen is loaded under a dead weight of 201 g-f (1.97 N) against the moving belt. The surface speed was held constant at 0.25 m/s and the test was stopped after set times to measure the width of the resulting cylindrical scar using a toolmaker's microscope at 40×. The cumulative test duration was 1 h of sliding.

The grindability tester was similar to the pin-on-belt configuration described in ASTM G 132 (Ref 7) except that the pin specimen remains stationary rather than being traversed laterally. It was developed in response to a need to measure the grindability of ceramics (Ref 8), and basically consists of a coolant-flooded abrasive belt on which a small test specimen, typically 3 × 4 mm in cross section and 50 mm long, is loaded end-on at a fixed surface speed (v) and normal force (L) for a set period of time (t). The specimen dimensions were originally selected based on those typical for ASTM flexure testing of ceramics (Ref 9). A broken flexure specimen could therefore also be used to test for the grindability of the material whose strength had previously been measured. The specimen remains in the same lateral location on the belt, so the time dependence of the grindability number can also be determined. The machine, shown schematically in Fig. 2, has automated loading cycle once the specimen is positioned above the belt.

The 50 mm wide belt was a commercial product consisting of 240 grit aluminum oxide particles. The applied load was 9.6 N and the sliding speed was set at 10 m/s. In all cases,

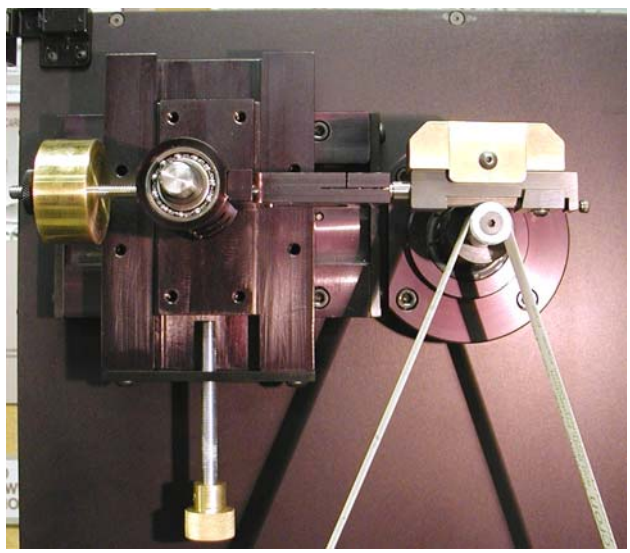

Fig. 1 Loop abrasion testing system. The specimen rests on the abrasive that drapes over a small pulley under a tared 200 g brass weight

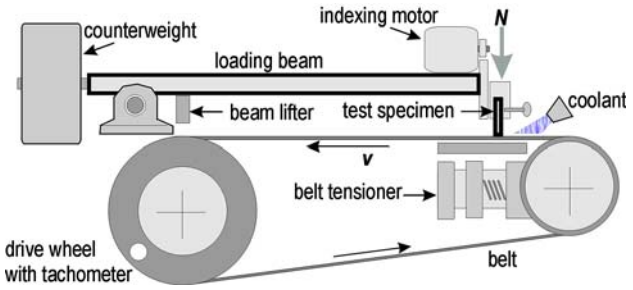

Fig. 2 Schematic of the grindability testing system used in this work. A timer raises and lowers the specimen, indexing it laterally between tests

water-based CIMTECH 500™ cutting fluid (1:20 dilution) was delivered by an immersion pump in the base of the unit. The sliding time was varied to study the effects of belt wear and loading. Typically, six to eight test tracks could be placed side-by-side on the same belt, and for every length change measurement, the specimen was translated laterally to a fresh portion of the belt. After mounting a new test piece, the grinding surface was worn in to achieve alignment with the belt, but that wear-in run was not recorded. The next run, after translating the specimen to a fresh spot, began the test series. The length change of the specimen (Δx) was measured using a precision digital micrometer mounted on the machine, and a grindability number Gr (in units of 10^{-4} mm^3/N·m), is calculated as follows:

$$Gr = \frac{ab(\Delta x)}{NL} \quad \text{(Eq 1)}$$

where a = length of the ground face, b = width of the ground face, N = the normal force, and L = sliding distance = vt. Gr is dimensionally same as the volumetric wear rate commonly reported in sliding wear studies. The numerator represents, in essence, the 'effect' of exposure to the belt and the denominator contains the applied conditions (the 'cause' of wear). From the standpoint of machinability, the higher the value for Gr, the easier the material is to remove under the stated conditions. Results of the current experiments will also indicate that, like full-size grinding behavior, Gr is time-dependent.

Surface grinding experiments were performed on the commercial CNC-controlled creep-feed grinder (K.O. Lee, VIGOR model), using the grinding conditions listed in Table 1. Grinding wheels were alumina (Norton 32A50-KVBE, 10 × 1 × 3), and the coolant was Cimtech™ 46C diluted (5% in water) using an approximately 5 gal/min (19 L/min) flow rate. The grinding wheel was dressed with a diamond point, without coolant, prior to use on each material. A witness specimen was ground with the freshly dressed wheel and measured using a stylus profiling system (Talysurf 120) to ensure proper dressing.

The grinder was instrumented using a 3-axis Kistler dynamometer stage and a spindle power sensor. Cutting force data was taken at three points in the experiment: at the beginning, halfway, and at the end. Each of the three data sets lasted about 32 s with a capture rate of 256 per second. At the beginning of each burst, the table was paused with the wheel out of contact so that the load cell could be zeroed. Before the first data was taken, however, coolant was allowed to flow over the specimen/load cell area in order to stabilize the temperature

Table 1 Grinding conditions

Parameter	Conventional units	Metric units
Wheel speed (clockwise)	2000 sf/min	10.2 m/s
Table speed	106 in./min	44.9 mm/s
Down feed (incremented at the operator's right side)	0.005 in./pass	0.0127 mm/pass
Total depth of material removed	0.100 in.	2.54 mm
Total volume removed from each specimen	0.169 in.^{3}	2765.3 mm^3

and reduce fluctuations in the output of the load cell. This stabilization procedure took up to an hour.

The initial size of grinding specimens was typically 9.53 (wide) × 114.3 (long) × 18 mm in height. The volume worn from of abrasive wheel was determined from the depth of the central region produced during grinding. Since the wheel was wider than the workpiece, the step height could be measured by grinding across a 3 mm thick machinable steel witness coupon. The grinding ratio, R_g, is defined as the ratio of volume of stock removed (V_{gs}) to the volume of wheel worn off (V_{gw}). The volume of the wheel was taken to be the product of the wear width, wheel circumference, and step height on the witness specimen.

The materials used in these tests and their selected mechanical and thermal properties are listed in Table 2. The Ti alloy was obtained through the courtesy of TIMET Corporation (Henderson, NV), and the composites were produced by special order from Dynamet Corporation (Burlington, MA). The microstructures of the materials are shown in Fig. 3(a-d). They represent a range of grain sizes and composite concentrations. The material in Fig. 3(d) is a blend of Ti-6Al-4V with 7.5% TiC with a binary alloy containing 7.5% W. It is said to offer the strength of Ti-6Al-4V but with enhanced ductility and the ability to be precipitation hardened. Vickers microindentation hardness (HV), scratch hardness (HS), and Brinell hardness (HBW) tests were also performed. HV tests used a load of 25 g-f, and the HS tests used a 400 g-f normal load and was conducted according to ASTM G 171 (Ref 10). Brinell hardness was obtained using a 500 kg-f load with a 10 mm WC ball in accordance with ASTM E10-07. These data are also given in Table 2.

3. Results

3.1 Low-Stress Abrasion

Each alloy was subjected to two ASTM G174 loop abrasion tests in which the wear scar width was measured periodically. Based on the width and length of the wear scar, and the radius of the upper pulley over which the abrasive loop traveled, the wear volume could be calculated. A plot of wear volume versus sliding distance of the specimen is shown in Fig. 4. Duplicate tests were quite repeatable and, therefore, plot symbols were the same for both tests of each material. Data seemed to fall in three groups: High wear for the Ti64 alloy, intermediate wear for the TiB_2 composite, and low wear for the other two composite materials that contained TiC. Data for the composites containing TiC fell so close together that there was no difference in loop abrasion resistance. Over the total test length of

Table 2 Compositions, designations, and selected properties of test materials. ($\underline{x}$ = average, σ = standard deviation)

Material ID	Composition/Preparation	Selected properties	$HV_{25\ gr}$, GPa	$HS_{400\ gr}$, GPa	HBW
Ti64	6.53 Al, 3.89 V, 0.035 Mo, 0.128 Fe, 0.02 Zr, 0.024 Si, 0.05 C, 0.181 O (a)	UTS = 953 MPa YS = 878 MPa Elongation = 12% HV_{2N} = 3.36 GPa k_{th} = 6.83 W/m·K ρ = 4.42 g/cm^3 (a)	$\underline{x}$ = 3.36 σ = 0.12	$\underline{x}$ = 3.35	$\underline{x}$ = 235.2 σ = 8.1
5TiB	Particle-reinforced composite produced by cold plus hot isostatic pressing (CHIP); 5 wt.% TiB_2	UTS = 1118 MPa YS = 1008 MPa Elongation = 3% k_{th} = 7.99 W/m·K ρ = 4.34 g/cm^3 (b)	Matrix material: $\underline{x}$ = 4.13 σ = 0.25	$\underline{x}$ = 3.97	$\underline{x}$ = 263.2 σ = 17.1
10TiC	Particle-reinforced composite produced by cold plus hot isostatic pressing (CHIP); 10 wt.% TiC	UTS = 987 MPa YS = 953 MPa El. = 1.5% k_{th} = 8.21 W/m·K ρ = 4.44 g/cm^3 (b)	Matrix material: $\underline{x}$ = 3.93 σ = 0.44	$\underline{x}$ = 3.89	$\underline{x}$ = 274.4 σ = 4.5
7.5W/TiC	Composite produced by cold plus hot isostatic pressing of powders (CHIP); Ti-7.5 wt.% W and Ti-6Al-4V with 7.5 wt.% TiC	UTS = 1022 MPa YS = 1015 MPa El. = 1% k_{th} = 6.57 W/m·K ρ = 4.68 g/cm^3 (b)	Matrix: $\underline{x}$ = 3.93 σ = 0.44 TiC particle: $\underline{x}$ = 25.4 σ = 5.0	$\underline{x}$ = 4.72	$\underline{x}$ = 286.1 σ = 1.9

(a) Heat composition and properties supplied by TIMET, Henderson, NV and (b) Mechanical properties provided by the supplier, Dynamet Corp., Burlington, MA; density and thermal conductivity were determined at Oak Ridge National Laboratory

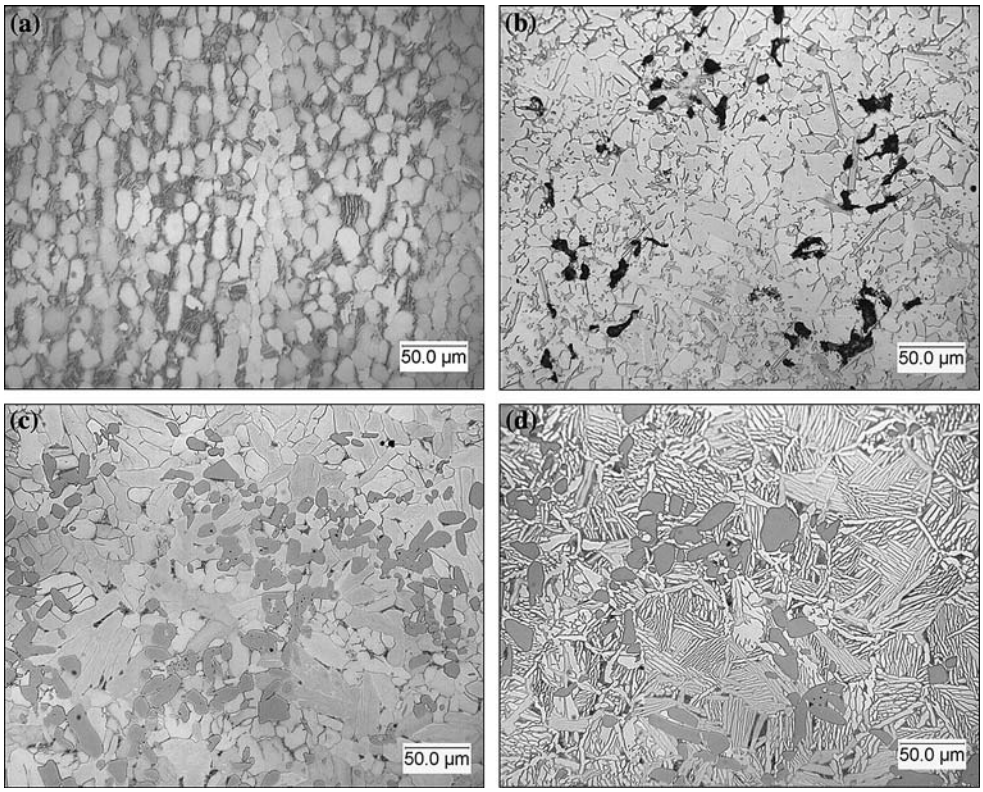

Fig. 3 (a) Ti-6Al-4V alloy, (b) Ti-6Al-4V with 5%TiB_2, (c) Ti-6Al-4V with 10%TiC, and (d) Ti-7.5W/7.5TiC (etched, light optical images)

approximately 60 min, the volume of material removed was linearly proportional to the sliding distance (or time), and, therefore, did not directly indicate that there was any loading of the belt, loss of grit particles, or wear of the grit. Unlike the high-stress belt test that uses the end of a square specimen, the contact area in the loop abrasion test increases with time as

the cylindrical wear scar grows; therefore, the load per unit area of contact decreases with time. The area of the scar A is the product of the arc of contact y and the specimen width c. Thus, for an abrasive loop draped over a pulley of radius R, and with a wear scar of length w, the contact area becomes:

$$A = cy = c\left(\frac{4\pi R\theta}{2\pi}\right) = 2cR\theta \qquad \text{(Eq 2)}$$

and θ (in radians) $= \sin^{-1}$ $(w/2R)$. The contact stress is approximately the load divided by the projected area of A. As data in Fig. 4 show, this decreasing stress effect did not seem to affect the volumetric wear rate significantly.

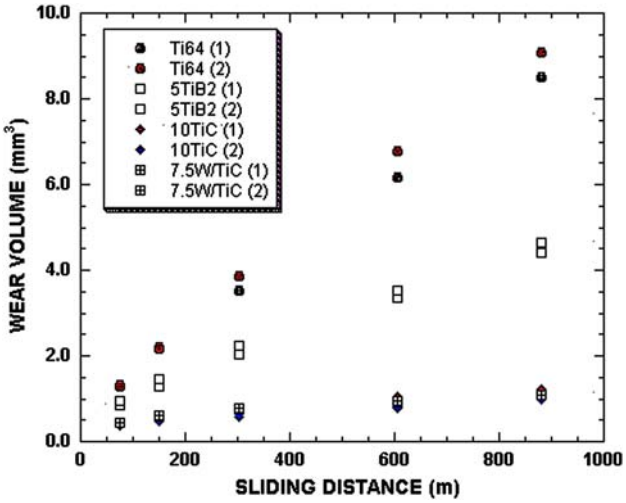

Fig. 4 Variation of abrasive wear volume with sliding distance for four Ti-based materials, each tested twice

Microstructural damage to the surfaces of loop abrasion test specimens is shown in Fig. 5(a-d). Backscattered electron imaging (BSE) of the composite enhanced the contrast between the hard particles and the matrix phase. The ductile behavior of the Ti64 is apparent from the wide continuous grooves. The abrasive marks in the composites are interrupted by the hard particles, and there are indications of particle fracture and pullout. The W-containing matrix alloy in Fig. 5(d) produces a more acicular appearance.

3.2 High-Stress Abrasion

Three coupons of each alloy were subjected to two belt abrasion tests with 10 and 20 s sliding durations. Grindability numbers *Gr*, which were computed using Eq 1, are given in Fig. 6. In general, the longer the exposure time, the lower the *Gr*, as might be expected from considerations of belt loading and abrasive grit wear. However, the *Gr* for the composites with higher loadings seem less affected by duration of belt grinding than the Ti64 and the $5TiB_2$.

Scanning electron micrographs of the faces of the grindability test specimens were obtained (see Fig. 7). In contrast to those for the loop abrasion test, the features were coarser with extensive evidence for plowing and tearing. The non-reinforced Ti64 (Fig. 7a) shows severe plastic deformation and tearing. In the composites, hard particles were fractured and pulled out, with some clusters of fragments remaining on the surface or trapped in cracks. In Fig. 7(d), some of the lamellar microstructural features prominent in Fig. 5(d) are covered with patches of sheared material that were formed by the plowing and shear processes of the grindability test.

Table 3 compares the relative loop abrasion response, grindability numbers, scratch hardness, Vickers microindentation hardness, and ultimate tensile strength for the composites

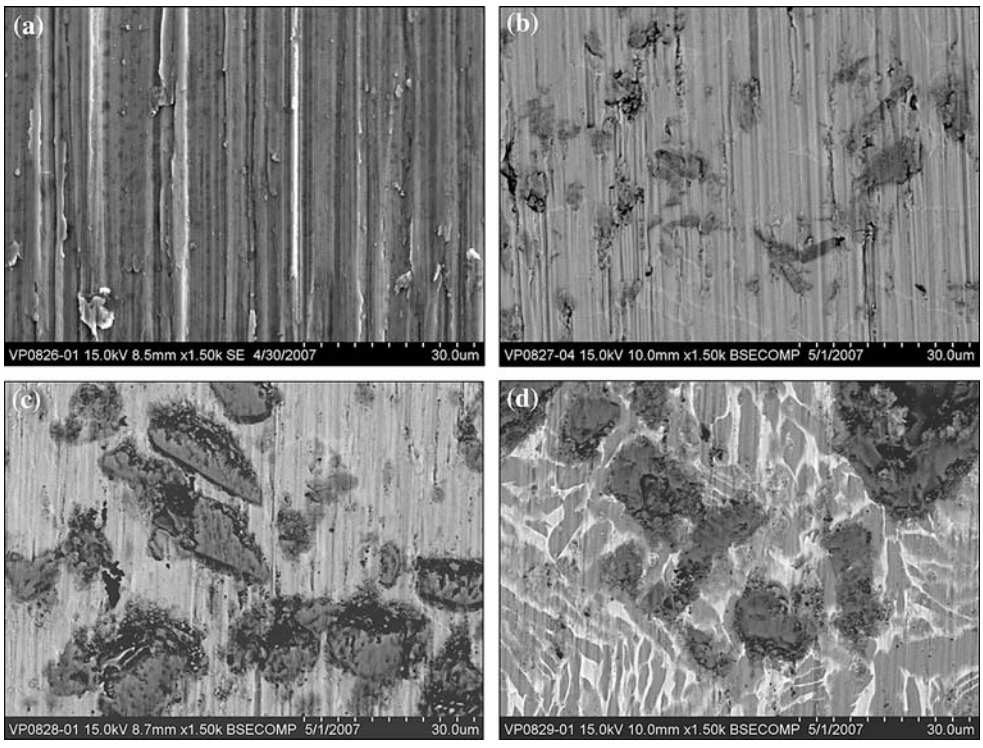

Fig. 5 Surfaces of loop abrasion test specimens. The abrasion direction is vertical (SEM)

to that of Ti64. Scratch hardness numbers show the $5TiB_2$ and 10TiC to be similar, but that does not reflect their performance in loop abrasion or grindability tests, where instead of a single sharp indenter, multiple contacts with fine abrasives occur. The low-stress, loop abrasion test does not distinguish between the bulk grindability to the extent that the high-stress belt-grinding test does. There is a modest comparative agreement between the relative Vickers hardness and the loop abrasion. It cannot be said that a strong correlation exists between the hardness data and the abrasion response, but rather the material ranking based on relative grindability matches that for the ultimate tensile strength (UTS) somewhat better. Thus, there seems to be a better correlation of grinding with bulk material properties than quantities based on localized measurements like single-point scratch hardness and quasi-static microindentation hardness. More importantly, these results suggest that HV and HS are not appropriate candidates for incorporation into a grinding model for these materials.

Plots of HBW against loop abrasion volume and grindability numbers are provided in Figs. 8 and 9, respectively. In both cases, a linear correlation (r^2) of better than 0.97 results. However, in both cases, there is a breakdown in the trend for the 7.5W/TiC composite. It is slightly harder than the 10TiC but more easily grindable and with more abrasive wear. In addition, the matrix alloy of the 7.5W/TiC was different in composition

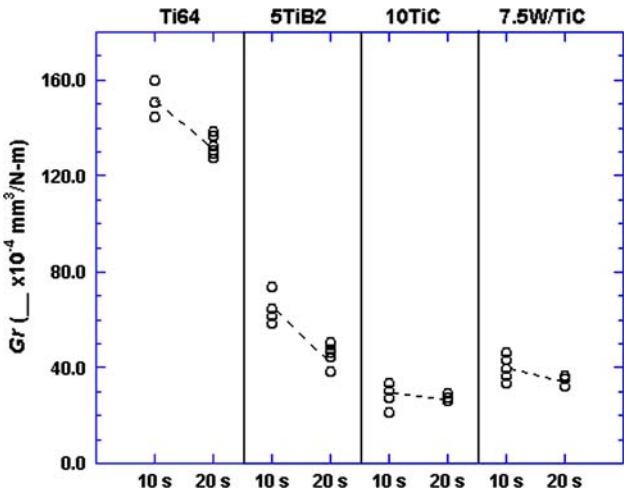

Fig. 6 Grindability numbers for four materials (6 data for each sliding time)

Table 3 Loop abrasion, grindability numbers, and hardness values of Ti-based composites relative to Ti64 (data compare the average of all measurements on a given material)

Characteristic	$5TiB_2$	10TiC	7.5W/TiC
Loop abrasion wear volume relative to Ti64 (full test length)	0.51	0.12	0.12
Gr relative to Ti64			
10 s sliding time	0.43	0.20	0.27
20 s sliding time	0.35	0.20	0.26
HS relative to Ti64	1.19	1.16	1.41
HV (matrix data) relative to Ti64	1.23	1.17	1.17
HBW relative to Ti64	1.12	1.17	1.22
UTS relative to Ti64	1.17	1.04	1.07

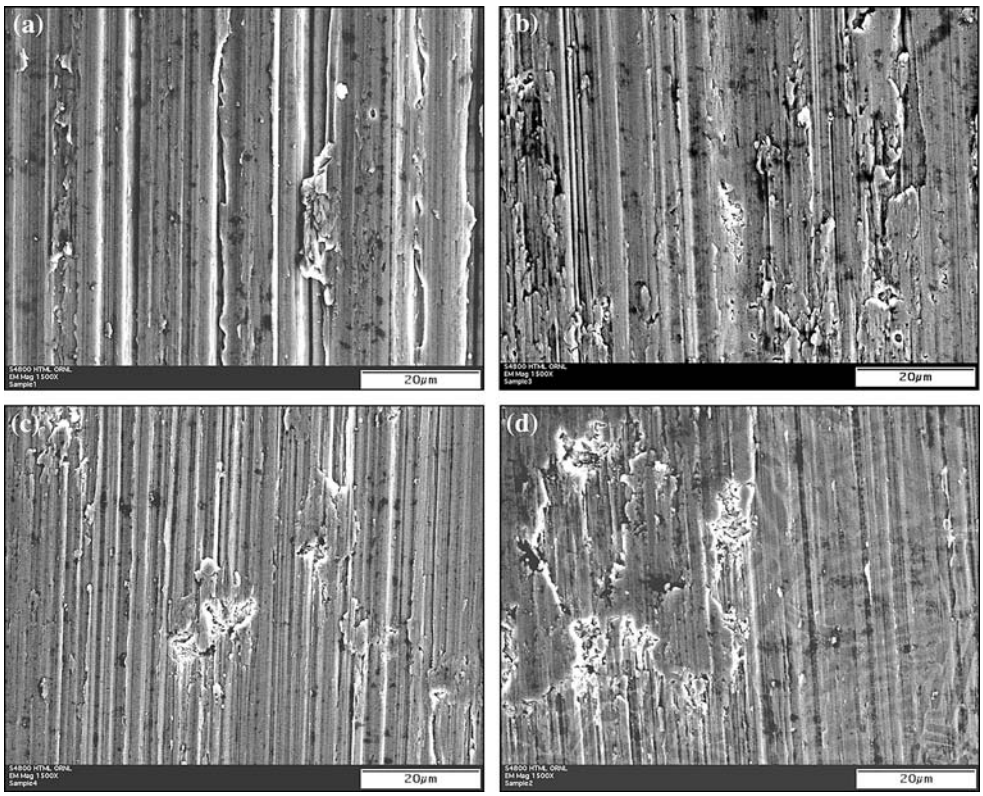

Fig. 7 Surfaces of coarse-ground specimens. The abrasion direction is vertical (SEM)

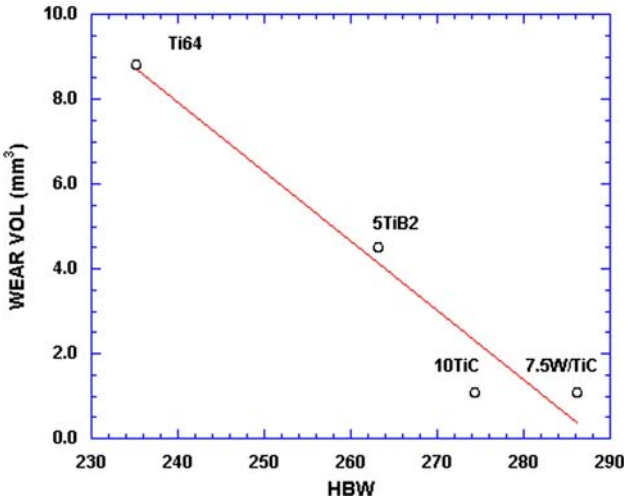

Fig. 8 Correlation between HBW and loop abrasion

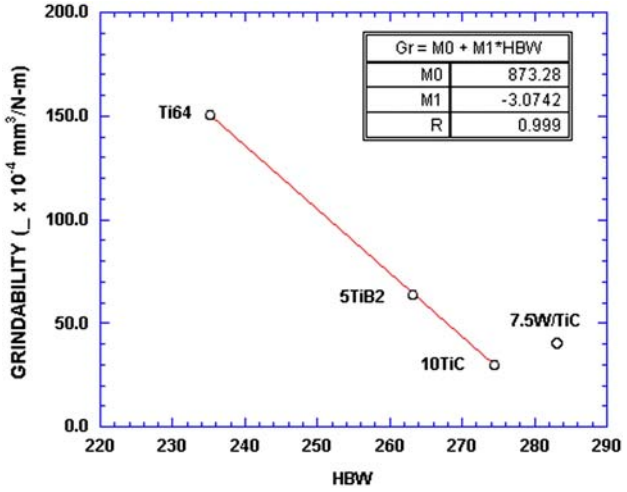

Fig. 9 Correlation between HBW and grindability number. Using the data for only the Ti-6Al-4V matrix materials indicates an excellent linear correlation

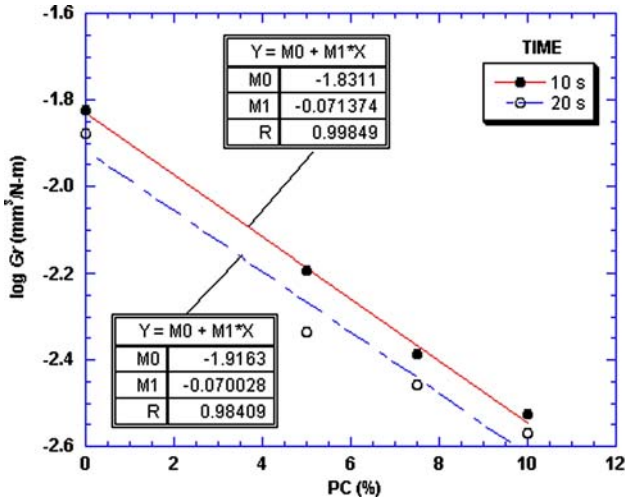

Fig. 10 Relationship between hard particle concentration (PC) and grindability of Ti alloys

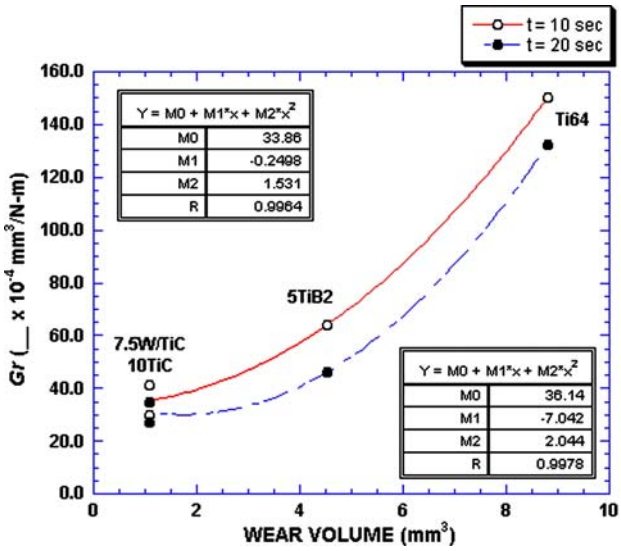

Fig. 11 Relationship between loop abrasion wear volume and belt grindability number for the same set of materials

than the other three, which were based on Ti64. If one were to look only at the bulk Ti64 and the two composites that used Ti64 matrices, the relationship in Fig. 9 would be strong.

A good correlation was observed between the log of the grindability number and the percent hard particles in the alloy, irrespective of whether they were TiB_2 or TiC and whether the matrix was Ti64 or had W additions (see Fig. 10). Data for both 10 s and 20 s of abrasion testing showed essentially the same relationship but with a slight offset. Therefore, one could write a general equation of the form:

$$\log Gr = M_0 + M_1\,(\mathrm{PC}) \qquad \text{(Eq 3)}$$

$$Gr = M_0\,(\mathrm{PC})^{M_1} \qquad \text{(Eq 4)}$$

The correlation of data between the loop abrasion test and the higher-stress grindability test was not linear. Figure 11 indicates a second-degree polynomial correlation between the wear volume from loop abrasion tests and grindability tests conducted for both 10 and 20 s. Under the current range of materials and test conditions, the correlation ($r^2 > 0.99$) looks quite good. Therefore, knowing either a grindability number or a loop abrasion wear volume for Ti alloys and composites it should, in principle, be possible to estimate the opposite quantity with good accuracy, other factors being equal. The reason why the correlation between the two test methods is not linear is likely to be affected at least in part by the contact geometry of the two tests. The GN test uses a rectangular test bar whose wear occurs as a decrease in length, but at constant contact area. One the other hand, the loop abrasion test involves the creation of a cylindrical arc of contact in which the nominal contact pressure decreases with time.

4. Surface Grinding Results

Wheel wear, grinding forces, and surface roughness data for the four Ti-based materials are summarized in Table 4. They include average and standard deviations of the grinding force in

Table 4 Results of surface grinding tests

	Ti64	5TiB$_2$	10TiC	7.5W/TiC
V_{gs} (mm^3) (a)	2765	2765	2765	2765
V_{gw} (mm^3)	559	606	1159	1393
R_g	4.94	4.56	2.39	1.98
F_x, initial – ave (std. dev.)	47.4 (7.6)	38.6 (5.1)	60.2 (6.9)	53.5 (8.0)
F_x, midway – ave (std. dev.)	40.7 (4.6)	37.1 (5.0)	45.6 (14.7)	46.5 (7.3)
F_x, end – ave (std. dev.)	40.0 (5.0)	38.9 (5.3)	42.4 (11.2)	45.8 (5.9)
Ave. F_x (init., mid., end)	42.7	38.2	49.4	48.6
F_n, initial – ave (std. dev.)	53.7 (5.9)	63.9 (8.0)	118.9 (10.0)	96.5 (8.8)
F_n, midway – ave (std. dev.)	54.3 (7.7)	55.8 (6.0)	94.0 (29.3)	77.8 (12.3)
F_n, end – ave (std. dev.)	49.7 (7.0)	55.3 (7.4)	85.3 (17.9)	90.4 (9.3)
Ave. F_n (init., mid., end)	52.6	58.3	99.4	88.2
(Ave. F_x/Ave. F_n)	0.81	0.66	0.50	0.55
Surface finish, R_a (μm)	1.68	1.04	0.86	1.04

V_{gs} = volume of stock removal; V_{gw} = volume of wheel worn off; R_g = grinding ratio; F_x = average tangential force during grinding; F_n = average normal force during grinding
(a) Established by specimen geometry and total depth removed

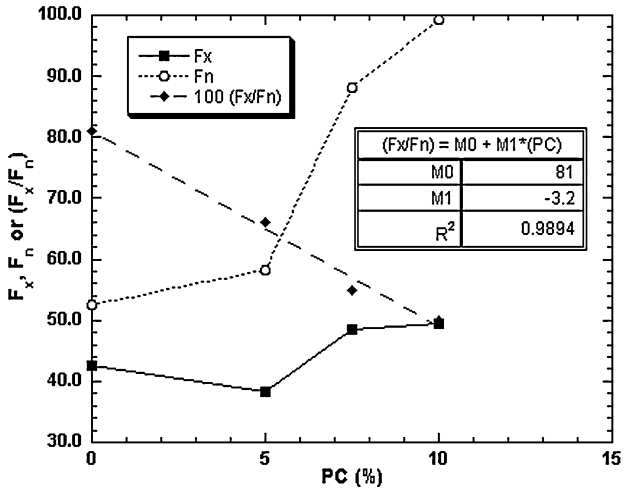

Fig. 12 Effects of hard particle concentration on grinding force

the tangential direction (F_x) and the normal direction (F_n) at the beginning, middle, and end of the run. The G-ratio (R_g) is determined by dividing stock volume removed by wheel wear volume. The lower the G-ratio, the more the wheel wears to remove a given volume of work material. As expected, the harder the work material, the more abrasive was removed during its machining, and the Ti64 had a G-ratio of nearly 5 while the harder composites had G-ratios a factor of about 2.5 lower.

In general, the higher the particle concentration, the higher was the average normal force, and except for the 5%TiB$_2$ alloy, the same trend was true for tangential force. Data show that the difference in composition between the alloys had a larger effect on F_n than on F_x. Figure 12 indicates the effect of particle concentration on the average values of F_n and F_x, but more interestingly on the ratio of F_x to F_n. The ratio was multiplied by 100 to enable its display on the same vertical axis as F_n and F_x. Individually, the relationship between normal or tangential force and particle concentration was not linear, but the (F_x/F_n) ratio bore a linear correlation, as indicated by inset in the figure. Therefore, hard particle content in this material system could be used to estimate either F_n or F_x if one of those two quantities were known.

5. Discussion

Microindentation and scratch hardness numbers were apparently too localized a measure of surface characteristics to correlate well with the grinding and abrasion response of the materials tested; therefore, their utility for grinding models is questionable. There was a better correlation of the behavior with Brinell hardness numbers, probably because the indentation displaces a larger volume of bulk material and thus can reflect both particle and matrix characteristics. In fact, as demonstrated in Fig. 8, the HBW correlated with abrasion data very well for the Ti64, 5TiB, and 10TiC, but it did not correlate quite as well with the 7.5W/TiC composite which had a different matrix composition. Therefore, while HBW provided a reasonable guide to predicting abrasion resistance and grindability within a composite having the same matrix and particle type, the trend determined for one matrix material might not extrapolate to particulate composites with other matrix compositions.

As shown in Fig. 11, there was a good correlation between loop abrasion and grindability test results. This might be expected because both are constant-load test methods, not displacement-controlled processes, as are most machining operations in which the forces depend on the depth of cut, infeed, and material. Since the two kinds of abrasion tests used different speeds, loads, and grit sizes, and the degree of abrasive wear and belt wear was not the same, the correlation between them was non-linear.

As might be expected, the higher the hard particle concentration, the larger were the grinding forces, with the normal force being most affected. Due to a ductile grooving material removal process (as exemplified by the abraded surfaces in Fig. 7), the Ti64 surface had the highest post-ground roughness, but all three composites had about the same final arithmetic average surface roughness after grinding, suggesting

that the higher grinding forces for the composites may have been due to the added work of pulling hard particles out of the matrix.

The interrelationships observed in the current study can serve as a guide to the development of surface grinding models for Ti-based alloys. For example, results showed that the particle concentration correlated well with the grinding forces that developed, and to a lesser extent to the finish of the ground surface.

The grinding ratios (R_g) shown in Table 4 seemed to be influenced not only by the hard particle concentration, but also by the matrix composition and particle type (TiB_2 versus TiC). Wheel wear volume greatly increased for TiC particles and for the W-strengthened matrix, and that leads to the argument that were another abrasive material than alumina used for grinding and abrasion tests, the interrelationships between the abrasion response and grinding parameters would have been different. The low R_G reported in Table 4 do not portend a very cost-effective process. G-ratios exceeding one hundred are desirable. The typical Knoop micro-indentation hardness of alumina is about 19-23 GPa, compared with 27-30 GPa for silicon carbide, 30-35 GPa for TiB_2, and still higher for superabrasives like cubic BN and diamond. It may be necessary to use a harder but more costly medium if an improved G-ratio trade-off with wheel cost is justified. Still, a limited set of surface grinding conditions was used in this work, and the authors do not claim that they were optimized for each material.

Additional research is needed to establish the applicability of the current results and relationships to abrasive media other than alumina, but having conducted this multiple cross-correlation suggests directions for future grinding research. Further studies are needed on the effects of particle content in titanium-based composites, the role of matrix composition on grindability, and the effects of the abrasive grit interactions on material removal rates for these composite materials.

6. Summary and Conclusions

Cross correlations were performed between several hardness tests, two abrasion tests, and surface grinding experiments on four titanium-based materials. The following conclusions were drawn:

1. For low-stress loop abrasion testing, the wear volume was linearly related to sliding time (distance) for all materials. Wear volume decreased with increasing particle concentration up to 7.5%, but there was no clear difference between the results for 7.5 and 10% TiC additions. Perhaps the difference in properties between the matrices of the 7.5% and 10% TiC composites compensated for particle concentration effects.
2. Data from two types of abrasive belt tests correlated better with Brinell hardness numbers (HBW) than with microindentation or scratch hardness numbers. In particular, there was a strong linear correlation of HBW with the grindability numbers for Ti-6Al-4V-based materials.
3. The normal force to tangential force ratio for surface grinding correlated with the particle content of the Ti composites. The higher the hard particle concentration, the lower was this grinding force ratio, suggesting that the resistance to material removal increased with particle content, as would be expected.
4. The grindability number had a second-degree polynomial relationship with the wear volume loss obtained using the low-stress loop abrasion test. Therefore, it was possible to relate loop abrasion data to the grindability data and, in turn, to the Brinell hardness number.
5. Grinding conditions were kept constant for the series of materials and were not optimized for each material. However, alumina wheel wear was high (and G-ratios were low), indicating a need to investigate a wider range of grinding conditions and media for specific Ti-based hard-particle composites.

Acknowledgments

The authors would like to thank J. McLaughlin and L. Walker, both from Oak Ridge National Laboratory, for their help on portions of this project. The reviews of Andrew Wereszczak and William Peter of ORNL are greatly appreciated, as is the advocacy and support of P. S. Sklad of ORNL. This work was support by the U.S. Department of Energy, Assistant Secretary for Energy Efficiency and Renewable Energy, Office of FreedomCAR and Heavy Vehicle Technologies, under contract DE-AC05-00OR22725 with UT-Battelle, LLC.

References

1. P.J. Blau, principal investigator, Cost-Effective Ceramic Machining Project, supported by the U.S. Department of Energy, Ceramic Technology Project, and managed by Oak Ridge National Laboratory, Oak Ridge, Tennessee, 1991–1996
2. F. Yang, B. Zhang, J. Wang, A. Zhu, and R. Monahan, The Effect of Grinding Machine Stiffness on Surface Integrity of Silicon Nitride, *J. Manuf. Sci. Eng.*, 2001, **123**(4), p 591–600
3. B. Zhu, C. Guo, J.E. Sunderland, and S. Malkin, Energy Partition to the Workpiece for Grinding of Ceramics, *Ann. CIRP*, 1995, **44**(1), p 267–271
4. T. Okabe, M. Kikuchi, C. Ohkubo, M. Koike, O. Okuno, and T. Oda, *Cost-Affordable Titanium*, F.H. Froes, M. Ashraf, and D. Fray, Eds., TMS, Warrendale, PA, 2004, p 177–181
5. K.W. Chan, M. Koike, and T. Okabe, Grindability of Ti Alloys, *Metall. Mater. Trans. A*, 2006, **37A**, p 1323–1331
6. "Standard Test Method for Measuring Abrasion Resistance of Materials by Abrasive Loop Contact," G 174-04, *Annual Book of ASTM Standards*, Vol. 03.02, ASTM 2006, p 718–724
7. "Standard Test Method for Pin Abrasion Testing," G 132-96, *Annual Book of ASTM Standards*, Vol. 03.02, ASTM 2006, p 542–549
8. C. Guo and R.H. Chand, "Cost-Effective Method for Determining the Grindability of Ceramics," Final report, ORNL Sub 93/SM036-1, Oak Ridge National Laboratory, Oak Ridge, TN, 1996, 90 pp
9. "Standard Test Method for Flexural Strength of Advanced Ceramics at Elevated Temperatures," C 1211-02, *Annual Book of ASTM Standards*, Vol. 15.01, ASTM, specimen configuration B
10. "Standard Test Method for Scratch Hardness of Materials Using a Diamond Stylus," G 171-03, *Annual Book of ASTM Standards*, Vol. 03.02, ASTM 2006, p 711–717